

Ground-state energy, density profiles, and momentum distribution of attractively interacting 1D Fermi gases with hard-wall boundaries: a Monte Carlo study

J. R. McKenney,^{1,*} C. R. Shill,^{1,†} W. J. Porter,^{1,‡} and J. E. Drut^{1,§}

¹*Department of Physics and Astronomy, University of North Carolina, Chapel Hill, NC, 27599, USA*

(Dated: September 27, 2018)

Motivated by the realization of hard-wall boundary conditions in experiments with ultracold atoms, we investigate the ground-state properties of spin-1/2 fermions with attractive interactions in a one-dimensional box. We use lattice Monte Carlo methods to determine essential quantities like the energy, which we compute as a function of coupling strength and particle number in the regime from few to many particles. Many-fermion systems bound by hard walls display non-trivial density profiles characterized by so-called Friedel oscillations (which are similar to those observed in harmonic traps). In non-interacting systems, the characteristic length scale of the oscillations is set by $(2k_F)^{-1}$, where k_F is the Fermi momentum, while repulsive interactions tend to generate Wigner-crystal oscillations of period $(4k_F)^{-1}$. Based on the non-interacting result, we find a remarkably simple parametrization of the density profiles of the attractively interacting case, which we generalize to the one-body density matrix. While the total momentum is not a conserved quantity in the presence of hard walls, the magnitude of the momentum does provide a good quantum number. We are therefore able to provide a detailed characterization of the (quasi-)momentum distribution, which displays rather robust discontinuity at the Fermi surface. In addition, we determine the spatially varying on-site density-density correlation, which in turn yields Tan's contact density and, upon integration, Tan's contact. As is well known, the latter fully determines the short-range correlations and plays a crucial role in a multitude of equilibrium and non-equilibrium sum rules.

PACS numbers: 03.65.Ud, 05.30.Fk, 03.67.Mn

I. INTRODUCTION

As is well-known, advances in trapping, cooling, and manipulation of ultracold atoms, single species and mixtures alike, have made it possible to realize controlled studies of quantum systems in strongly coupled few- and many-body regimes [1]. The already large set of possibilities allowed by those experimental techniques continues to expand further and faster than ever. Understanding strongly coupled quantum matter in these atomic systems, in the wide variety of available scenarios, is of broad interest: strongly correlated matter is a challenging problem that pervades all energy scales, from quantum chromodynamics to condensed matter physics.

One of the most fruitful exchanges has actually been with the area of nuclear and neutron matter structure. In the latter, interactions are of limited range, and scattering lengths are comparatively large, a situation that bears strong similarities with ultracold atomic fermions close to a Feshbach resonance, differences notwithstanding [2]. Similarly, the realization of periodic systems via optical lattices [3] and the creative approach to engineering topologically non-trivial phases using internal degrees of freedom [4] have recently strengthened the connections to condensed matter physics.

New experimental techniques allow for the implemen-

tation of (quasi-) hard-wall traps. This development is interesting because the “flat-bottom” of the trap simulates a uniform system [5]. Close to the boundaries, or for low particle numbers, the edge effects result in the so-called Friedel oscillations, i.e. deviations from uniformity. The original work by Friedel actually considered the problem of the density variations due to the presence of an impurity [6] in an electronic system. Since then, other authors considered similar “impurity” problems (see e.g. [7–9]), and more recently the application of Friedel oscillations as probes for quasiparticles has been advocated [10].

In addition to the above, there are other motivations to understand Friedel oscillations in detail. For instance, it was shown by Zhang et al. in Ref. [11] that the presence of boundaries and interfaces in nanocomposites and heterostructures limits their mechanical strength precisely due to the appearance of Friedel oscillations. Clark et al. [12] showed that Friedel oscillations near a bilayer-monolayer graphene interface open a gap at the Fermi energy (for electrons with wave vectors normal to said interface), which consequently affects transport properties across the boundary. The interplay between the shape of the Fermi surface and Friedel oscillations (in particular for an oxygen impurity on the surface of a ferromagnetic thin film) was studied by Bouhassoune et al. [13], where “giant” directional effects were reported and shown to be tunable, with consequences for nanospintronics applications. Generally speaking, Friedel oscillations continue to be of interest to solid-state physics and materials science, even though their existence has been qualitatively understood for a while.

* joshmck@unc.edu

† crshill@live.unc.edu

‡ wjporter@live.unc.edu

§ drut@email.unc.edu

In this work, we do not consider impurities *per se*, but treat the problem of density oscillations resulting from “open” or “hard-wall” boundary conditions in a non-relativistic system of spin-1/2 fermions. Previous work studied this problem in the electronic case using bosonization [14, 15] or a variety of numerical methods [16–20]. Using bosonization and density-matrix renormalization group (DMRG) techniques, Ref. [21] studied a related situation, namely the *repulsive* Hubbard model in 1D with hard-wall boundaries. It was then found that the repulsive interaction parametrizes a crossover between Friedel-type density oscillations (characterized by a $2k_F$ wavelength) at weak coupling and Wigner-crystal-type oscillations (with $4k_F$ wavelength) at strong coupling. In the latter regime, the repulsion forces particles of opposite spins to occupy higher momentum states, effectively doubling the Fermi momentum.

As mentioned above, here we quantitatively explore several properties of spin-1/2 fermions in 1D with *attractive* short-range interactions confined by hard-wall boundaries. We calculate density profiles and study the enhancement of Friedel oscillations with increasing interaction strength; determine the occupation of standing-wave orbitals; and find the ground-state energy. In addition, we present a detailed characterization of the one-body density matrix and the short-distance correlations by computing the so-called contact density [22], which in these systems is a spatially varying quantity. As is well known, the contact fully characterizes the short-distance behavior of correlations and enters sum rules of transport coefficients (see e.g. [23]). We study all of the above in the few- to many-body range of $N = 8, \dots, 24$ unpolarized particles and cover weakly to strongly coupled regimes, as measured by the conventional dimensionless coupling γ (see below).

Naturally, our work complements Ref. [21] mentioned above in that we study the regime of attractive interactions, but we also expand on that work by considering a range of particle numbers. In contrast to the repulsive case, strong pairing correlations induced by attractive interactions lead to two-body bound-state formation and an enhancement of the Friedel oscillations, with a characteristic coupling-dependent discontinuity in the momentum distribution. The effect on Friedel oscillations was also noted in Ref. [24], where a similar calculation was carried out in the presence of a harmonic trapping potential (see also Ref. [25]).

Our calculations are also a first step towards exploring the properties of analogue systems in higher dimensions. As outlined in Ref. [26], this is enabled by Fourier acceleration, which can be adapted to hard-wall boundaries without affecting the dominant scaling of computational cost with system size. The same methods can be applied to systems in optical lattices, in particular in cases of internal degeneracies $N_f > 2$.

Generally speaking, correlations tend to be stronger in 1D systems than in their 2D and 3D counterparts [27].

For this reason, investigating and implementing non-perturbative methods [such as exact diagonalization, quantum Monte Carlo (QMC), density-matrix renormalization group (DMRG), Bethe ansatz (BA), bosonization, etc.] are essential. However, not all of these methods are universally applicable. For instance, quantum Monte Carlo can address problems in any number of spatial dimensions, but suffers from a sign problem at finite polarization and for repulsive interactions. The BA can solve the problem exactly for attractive or repulsive short-range interactions in 1D, and it has been widely applied for infinite systems (see e.g. Ref. [28]). The BA is not applicable in higher dimensions or in the presence of external trapping potentials, as translation invariance is broken, but it can and has been applied to 1D infinite square-well traps with repulsive interactions [29]. The DMRG method has also been used to analyze that system [20]. Finally, bosonization methods are often restricted to very low temperatures where the dispersion relation around the Fermi points can be well approximated as linear. As argued in Ref. [30], however, it has become clear in the last few years that considering non-linearities is important, as they account for characteristic behavior even at the level of broad, qualitative features, most noticeably so in the system’s dynamic response functions [31]. For these reasons, there have recently been a number of exact diagonalization (and similar) studies, with focus on pairing correlations in spin-polarized, harmonically trapped systems (see e.g. Refs. [32–35]). The same reasons further motivate the present work.

II. MANY-BODY METHOD

A. Hamiltonian and basic formalism

In this work we will focus on a non-relativistic Hamiltonian \hat{H} , with short-range interactions, as a model relevant for matter in dilute regimes. Thus,

$$\hat{H} = \hat{T} + \hat{V}, \quad (1)$$

where

$$\hat{T} = \sum_{s=\uparrow,\downarrow} \int_0^L dx \hat{\psi}_s^\dagger(x) \left(-\frac{\hbar^2 \partial_x^2}{2m} \right) \hat{\psi}_s(x) \quad (2)$$

is the kinetic energy, and

$$\hat{V} = -g \int_0^L dx \hat{n}_\uparrow(x) \hat{n}_\downarrow(x), \quad (3)$$

is the two-body, zero-range interaction. Although we have written \hbar and m explicitly above, we will take them to unity from this point on and similarly for Boltzmann’s constant k_B . While g is the bare coupling, it is physically meaningful in 1D: $g = 2/a_0$, where a_0 is the scattering length. As conventional in studies of uniform systems,

we define a dimensionless coupling

$$\gamma \equiv \frac{gL}{N}, \quad (4)$$

where L is the physical extent of the system and N is the total particle number.

As in previous work [36], we approach the ground state of our many-body quantum system by imaginary-time evolution of a “guess” state $|\psi_0\rangle$

$$|\psi\rangle_\beta = e^{-\beta\hat{H}} |\psi_0\rangle, \quad (5)$$

where β is the extent of the imaginary time evolution. This approach is feasible if the guess has a non-vanishing projection onto the true ground state. We take $|\psi_0\rangle$ to be a Slater determinant of single-particle orbitals $\{\varphi_k\}$ given by plane waves with hard-wall boundary conditions, i.e.

$$\varphi_k(x) = \sqrt{\frac{2}{L}} \sin\left(\frac{\pi k x}{L}\right), \quad (6)$$

where L is the size of the box, and k is a positive integer. More specifically, we take $k = 1, 2, \dots, N_\uparrow$ with $N_\uparrow = N_\downarrow = N/2$ being the number of fermions of each species. In this method, it is essential to have access to the operator

$$\hat{U}(t', t) \equiv \exp\left[-(t' - t)\hat{H}\right], \quad (7)$$

which is a complicated object in general, but which can be approximated using a Suzuki-Trotter decomposition

$$\hat{U}(t + \tau, t) = e^{-\tau\hat{T}/2} e^{-\tau\hat{V}} e^{-\tau\hat{T}/2} + O(\tau^3), \quad (8)$$

where τ is our imaginary-time discretization parameter. This factorization allows us to use, at each time step t , an auxiliary-field Hubbard-Stratonovich transformation of the interaction, i.e. a representation of the two-body interaction via one-body potentials:

$$e^{-\tau\hat{V}} = \int \mathcal{D}\sigma(x) e^{-\tau\hat{V}_{\uparrow,\sigma}} e^{-\tau\hat{V}_{\downarrow,\sigma}}, \quad (9)$$

where the $\hat{V}_{s,\sigma}$ are external-potential, one-body operators that depend on the auxiliary field $\sigma(x)$. The integral $\int \mathcal{D}\sigma(x)$ is a sum over all possible configurations of σ at the specific time t [see Eq. (8)].

Combining the above steps, one finds

$$\hat{U}(\beta, 0) = \int \mathcal{D}\sigma(x, t) \prod_t \hat{U}_\sigma(t + \tau, t), \quad (10)$$

where the path integral is over all possible spacetime dependent fields $\sigma(x, t)$ and the σ -specific evolution operator is

$$\hat{U}_\sigma(t + \tau, t) \equiv e^{-\tau\hat{T}/2} e^{-\tau\hat{V}_{\uparrow,\sigma}} e^{-\tau\hat{V}_{\downarrow,\sigma}} e^{-\tau\hat{T}/2}, \quad (11)$$

which is a product of exponentials of one-body operators.

Moreover, we identify a zero-temperature partition sum

$$\mathcal{Z} \equiv \langle \psi_0 | \hat{U}(\beta, 0) | \psi_0 \rangle = \int \mathcal{D}\sigma(x, t) P[\sigma], \quad (12)$$

where we defined

$$P[\sigma] \equiv \langle \psi_0 | \hat{U}_\sigma(\beta, 0) | \psi_0 \rangle. \quad (13)$$

Since \hat{U}_σ is composed of a string of exponentials of one-body operators, a well-known result of second-quantization formalism indicates that (assuming our guess state $|\psi_0\rangle$ is a single Slater-determinant state, as specified above)

$$P[\sigma] = \langle \psi_0 | \hat{U}_\sigma(\beta, 0) | \psi_0 \rangle = \det^2 [M_\sigma(\beta)], \quad (14)$$

where the power of two results from our system having two distinguishable (but otherwise identical) fermion species. The matrix $M_\sigma(\beta)$ is the one-particle representation of $\hat{U}_\sigma(\beta, 0)$, restricted to the Hilbert space of the occupied orbitals, i.e.,

$$[M_\sigma(\beta)]_{ab} = \langle a | \hat{U}_\sigma(\beta, 0) | b \rangle, \quad (15)$$

where $a, b = 1, 2, \dots, N_\uparrow$. Using this auxiliary field formalism, one may sample σ according to $P[\sigma]$ using well-known methods. For the calculations carried out in this work, we used the lattice hybrid Monte Carlo algorithm [37, 38].

B. Expectation values of operators

The above formalism enables the non-perturbative evaluation of arbitrary observables, as long as $P[\sigma]$ is non-negative (which in our case it is, as mentioned above), as we shall see next. The ground-state expectation value of an operator \hat{O} is

$$\langle \hat{O} \rangle = \lim_{\beta \rightarrow \infty} O_\beta, \quad (16)$$

where

$$O_\beta \equiv \frac{\langle \psi_0 | \hat{U}(\beta, \beta/2) \hat{O} \hat{U}(\beta/2, 0) | \psi_0 \rangle}{\langle \psi_0 | \hat{U}(\beta, 0) | \psi_0 \rangle}. \quad (17)$$

Once the time-evolution operators \hat{U} are written in field-integral form, as shown in the previous subsection, Eq. (17) becomes

$$O_\beta = \frac{1}{\mathcal{Z}} \int \mathcal{D}\sigma P[\sigma] O[\sigma], \quad (18)$$

where

$$O[\sigma] \equiv \frac{\langle \psi_0 | \hat{U}_\sigma(\beta, \beta/2) \hat{O} \hat{U}_\sigma(\beta/2, 0) | \psi_0 \rangle}{\langle \psi_0 | \hat{U}_\sigma(\beta, 0) | \psi_0 \rangle}. \quad (19)$$

This path integral form Eq. 18 is a function of the imaginary time β , which should approach the ground-state answer when extrapolated to large β (see Fig. 1).

In practice, the calculation of $O[\sigma]$ above, for a given configuration of the field σ , can be easily carried out when \hat{O} is generic one-body operator, in the following fashion. Going back to Eqs. (12)-(15), we insert a source factor $\exp(\lambda\hat{O})$ as follows; we take

$$\langle \psi_0 | \hat{U}_\sigma(\beta, 0) | \psi_0 \rangle \rightarrow \langle \psi_0 | \hat{U}_\sigma(\beta, \beta/2) e^{\lambda\hat{O}} \hat{U}_\sigma(\beta/2, 0) | \psi_0 \rangle \quad (20)$$

Since the source factor is the exponential of a one-body operator, it modifies the form of M_σ defined above in a predictable way. Inserting the resulting expression in Eq. (12) (or rather its natural logarithm), differentiating with respect to λ , and taking $\lambda = 0$, it is easy to identify

$$O[\sigma] = \text{tr}[M_\sigma^{-1} U_\sigma(\beta, \beta/2) O U_\sigma(\beta/2, 0)], \quad (21)$$

where the trace is over the space of occupied orbitals, and $U_\sigma(t, t')$ and O are the single-particle matrix representations of $\hat{U}_\sigma(t, t')$ and \hat{O} , respectively. Note, in particular, that the matrix product of U_σ and O above is over the full single-particle space, not just the occupied orbitals.

III. RESULTS

Using the formalism presented above, we carried out lattice calculations in fixed system sizes of length $L = (N_x + 1)\ell$, discretized by setting $N_x = 20, 30, 40, 60, 80$ and maintaining L constant. Below we present plots for several quantities for $N_x = 80$, and discuss finite-size effects in a later section. The extent of the time direction, as measured by the dimensionless parameter $\beta\varepsilon_F$, was varied so as to allow for a meaningful extrapolation to the ground state, as explained below. Here, $\varepsilon_F = k_F^2/2$, and

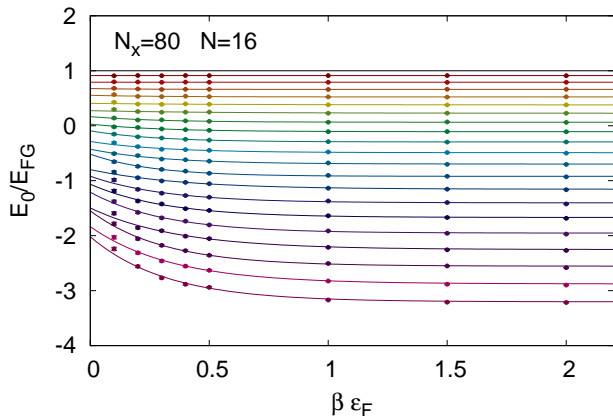


FIG. 1. Convergence of our energy estimator as a function of $\beta\varepsilon_F$, for $N = 16$ particles in a 1D segment (discretized using $N_x = 80$ points), for couplings $\gamma = 0.0, 0.2, \dots, 4.0$ (top to bottom).

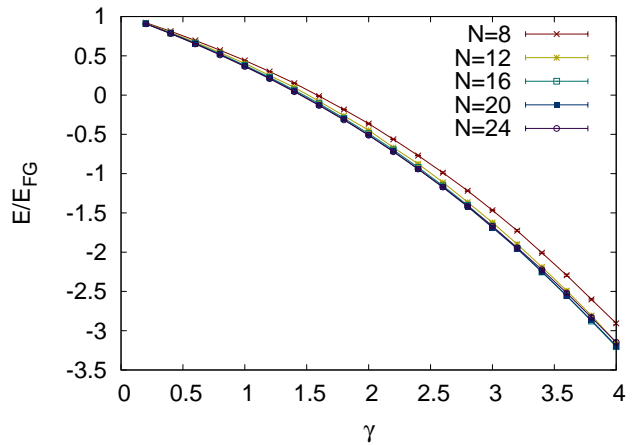


FIG. 2. The ground-energy of $N = 8, \dots, 24$ unpolarized fermions in a 1D segment (discretized using $N_x = 80$ points), in units of its non-interacting counterpart E_{FG} , as a function of the dimensionless coupling γ .

$k_F = \pi N/(2L)$, where N is the total particle number. In such lattices, we studied systems of $N = 8, 12, \dots, 24$ particles by taking 10^4 samples of the auxiliary field, which yields statistical uncertainties on the order of 1%. Finally, we varied the strength of the interaction between $\gamma = 0$ and $\gamma = 4.0$.

A. Ground-state energy

In order to determine the ground-state energy we used the formalism presented in the previous section, but used a shortcut: the β derivative of the path-integral form of $\ln \mathcal{Z}$ produces the desired expression, up to a constant. It is not difficult to show (see Ref. [37]) that the resulting estimator E_β approaches the ground-state result E_{GS} exponentially, i.e.

$$E_\beta \equiv -\frac{\partial \ln \mathcal{Z}}{\partial \beta} \rightarrow E_{GS} + K e^{-\beta\Delta}, \quad (22)$$

where K is a constant and Δ is the difference between the energy of the first excited state and the ground state. In Fig. 1 we show the above exponential fits to Monte Carlo data for a representative case ($N_x = 80$, $N = 16$) for several couplings.

In Fig. 2, we show our results for the ground-state energy E_{GS} in units of the energy of the non-interacting case

$$E_{FG} = \frac{\pi^2}{L^2} \sum_{k=1}^{N/2} k^2 = \frac{\pi^2}{24L^2} N(N+1)(N+2). \quad (23)$$

As is evident from the figure, for all the couplings we studied, the ground-state energy appears to approach the large- N limit very quickly.

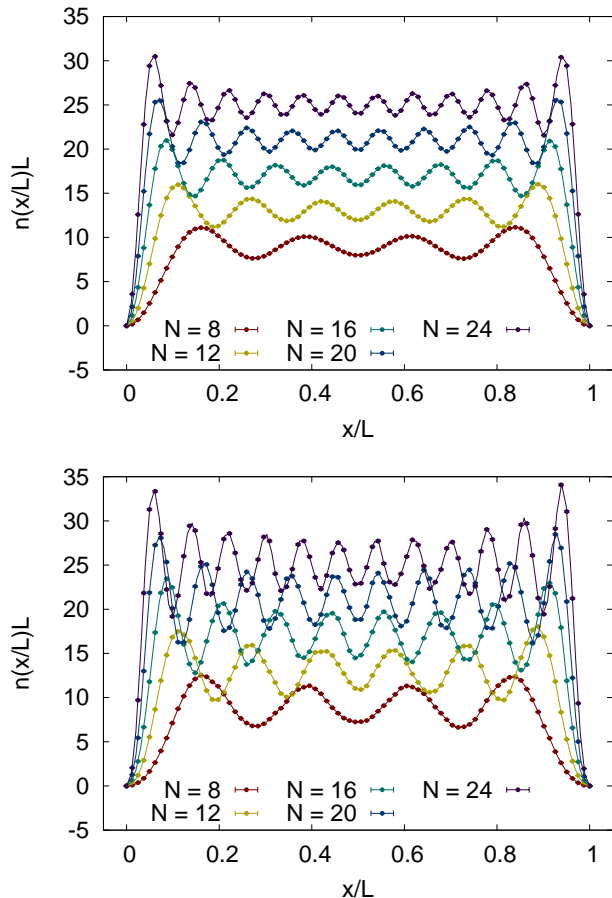


FIG. 3. Density profiles versus the scaled position x/L for $N_x = 80$ at weak coupling ($\gamma = 0.2$, top panel) and strong coupling ($\gamma = 3.0$, bottom panel), for particle numbers $N = 8, 12, 16, 20, 24$ (from bottom to top).

B. Density profiles

To calculate the density profiles we used the expression of Eq. (21), where $\hat{O} = \hat{n}(x)$, which indicates that

$$n(x) = \langle \hat{n}(x) \rangle = \frac{1}{Z} \int \mathcal{D}\sigma P[\sigma] n[\sigma, x], \quad (24)$$

where

$$n[\sigma, x] \equiv \sum_{a,b,c}^{N/2} [M_\sigma^{-1}]_{ab} [U_\sigma(\beta, \beta/2)]_{bx} [U_\sigma(\beta/2, 0)]_{xa} \quad (25)$$

To derive the previous expression, we have used that the single-particle representation of $\hat{O} = \hat{n}(x)$ is simply $O_{y,y'} = \langle y | \hat{n}(x) | y' \rangle = \delta(y, y') \delta(x, y)$, where $|y\rangle$ is a coordinate eigenstate.

In Fig. 3 we show the density profiles for two different values of the attractive coupling γ as a function of particle number N . As is evident from the figure, the main effect of attractive interactions is to enhance the amplitude of the Friedel oscillations while their frequencies are

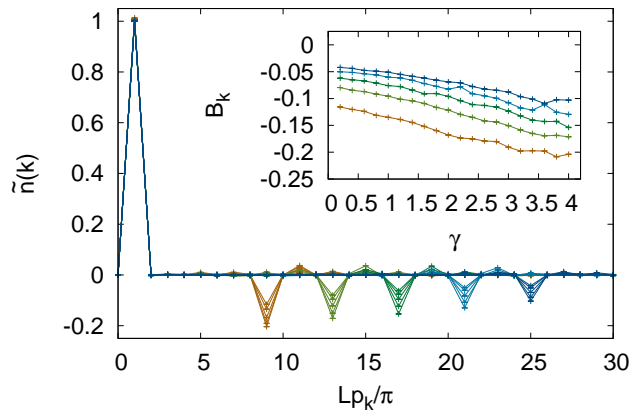


FIG. 4. Hard-wall transform coefficients B_k of Eq. (27), as a function of $Lp_k/\pi = k$, for $N_x = 80$ and several values of the coupling γ and particle number N . Note the maximum at $k = 1$ is equal to unity to an accuracy better than 2% for all γ and N ; the minima, on the other hand, show clear variation with increasing $N = 8, \dots, 24$ (left to right) as well as increasing γ (top to bottom; see inset). Inset: Value of the minimum as a function of the coupling γ for $N = 8, \dots, 24$ (bottom to top).

maintained. In order to analyze the oscillations in more detail, we recall that the density profile of the noninteracting case can be easily obtained by summing the contributions of the $N/2$ occupied single-particle states, namely

$$\begin{aligned} n(x/L) &= \frac{2}{L} \sum_{k=1}^{N/2} \sin^2 \left(\frac{\pi k x}{L} \right) \\ &= \frac{N+1}{L} - \frac{1}{L} \frac{\sin \left(\frac{\pi(N+1)x}{L} \right)}{\sin \left(\frac{\pi x}{L} \right)}, \end{aligned} \quad (26)$$

where L is the physical size of the box. To analyze the interacting density profiles, we rewrite the above as

$$\begin{aligned} \frac{L}{N+1} n(x/L) \sin \left(\frac{\pi x}{L} \right) &= \sin \left(\frac{\pi x}{L} \right) - \frac{1}{N+1} \sin \left(\frac{\pi(N+1)x}{L} \right) \\ &= \sum_{k=1}^{N_x} B_k \sin \left(\frac{\pi k x}{L} \right) \equiv \tilde{n}(x/L), \end{aligned} \quad (27)$$

where we have used a general Fourier expression obeying hard-wall boundary conditions in the last equality. Obviously, the noninteracting system satisfies $B_k = 0$ for all k except the cases of $B_1 = 1$ and $B_{N+1} = -1/(N+1)$. Note that the multiplication by $\sin(\frac{\pi x}{L})$ necessarily obliterates any information at $x = 0$, but we already know that the density vanishes at that point.

In Fig. 4 we show the coefficients B_k as a function of k and the coupling strength, for a representative case. The dominant contributions are always at $k = 1$ and $k = N + 1$, regardless of the strength of the coupling.

This is a remarkably clean signal that can be experimentally verified and which is especially surprising in light of bosonization analyses. The latter indicate that the denominator $\sin(\pi x/L)$ should appear elevated to a non-trivial power (i.e. different from unity) that is directly related to the parameters of the low-energy effective theory (see e.g. Ref. [21]).

The physical origin of the $k = 1$ and $k = N + 1$ peaks can be gleaned from the non-interacting result Eq. (26). The former provides the “overall” or “average” density in the bulk and is responsible for (all but one of) the particle number count; it therefore survives in the thermodynamic limit. The second term (and presumably every other non-vanishing term in the interacting case) is associated with the physics at the Fermi surface.

C. One-body density matrix

In order to characterize the one-body density matrix in an efficient way, we perform a more general version of the spectral analysis previously applied to the density profile. The non-interacting one-body density matrix may be computed trivially by collecting contributions from the $N/2$ occupied orbitals:

$$\begin{aligned} G_1(x, x') &= \frac{2}{L} \sum_{k=1}^{N/2} \sin\left(\frac{\pi k x}{L}\right) \sin\left(\frac{\pi k x'}{L}\right) \\ &= \frac{1}{2L} \left[\frac{\sin\left(\frac{\pi(N+1)(x-x')}{2L}\right)}{\sin\left(\frac{\pi(x-x')}{2L}\right)} - \frac{\sin\left(\frac{\pi(N+1)(x+x')}{2L}\right)}{\sin\left(\frac{\pi(x+x')}{2L}\right)} \right]. \end{aligned} \quad (28)$$

Again, we rewrite the above as (for $x \neq x'$)

$$\begin{aligned} 2LG_1(x, x') &\sin\left(\frac{\pi(x-x')}{2L}\right) \sin\left(\frac{\pi(x+x')}{2L}\right) \\ &= \sin\left(\frac{\pi N x}{2L}\right) \sin\left(\frac{\pi(N/2+1)x'}{L}\right) \\ &\quad - \sin\left(\frac{\pi(N/2+1)x}{L}\right) \sin\left(\frac{\pi N x'}{2L}\right) \\ &= \sum_{k=1}^{N_x} \sum_{k'=1}^{N_x} B_{kk'} \sin\left(\frac{\pi k x}{L}\right) \sin\left(\frac{\pi k' x'}{L}\right) \\ &\equiv \tilde{G}_1(x, x'), \end{aligned} \quad (29)$$

where we see that $B_{kk'} = 0$ for all k, k' except for the cases of $B_{\frac{N}{2}, \frac{N}{2}+1} = -B_{\frac{N}{2}+1, \frac{N}{2}} = 1$, corresponding to k_F and the first excited state above the Fermi level. Note that the antisymmetry in the coefficients was introduced in Eq. (29) via the antisymmetry in x and x' .

Interestingly, the non-zero $B_{kk'}$ in the non-interacting case display the property that $|k - k'| = 1$ and $k + k' = N + 1$, reflecting the same wavelengths observed in the spatial density profile, $n(x)$. As seen in Fig. 5 (top), in the presence of attractive interactions, amplitude from $B_{\frac{N}{2}, \frac{N}{2}+1}$ and its antisymmetric partner appears to shift

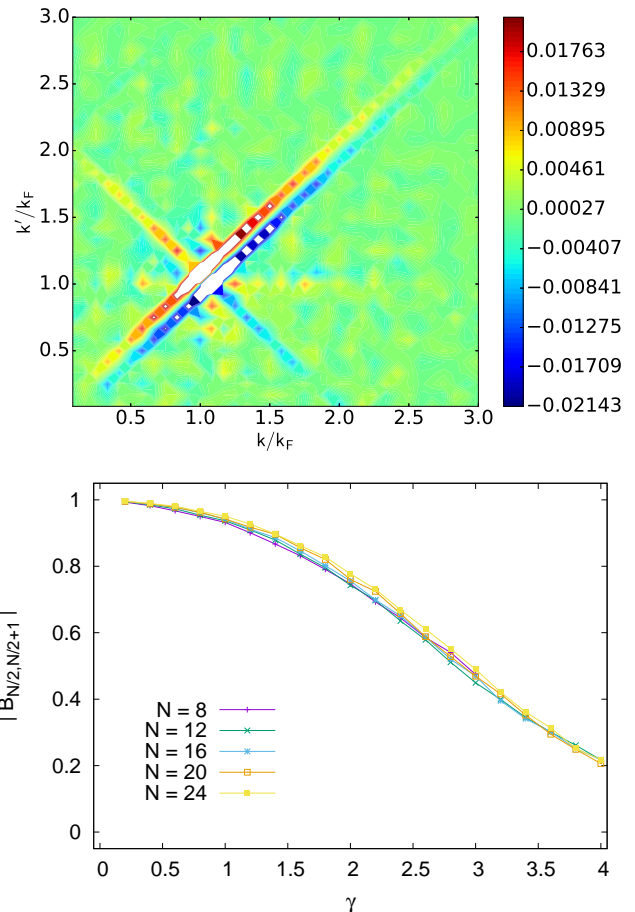


FIG. 5. Top: Hard-wall transform coefficients $B_{k,k'}$ of Eq. (29), as a function of $k = Lp_k/\pi$ and $k' = Lp_{k'}/\pi$, for $N_x = 80$, $\gamma = 4.0$, and $N = 24$. Bottom: Amplitude variation of the main peak $B_{\frac{N}{2}, \frac{N}{2}+1}$ as a function of γ for several particle numbers.

to neighboring modes, which continue to obey the same relations for $|k - k'|$ and $k + k'$. This decay of the main peak is enhanced as γ is increased, as Fig. 5 (bottom) demonstrates.

D. Quasi-momentum distribution

In translationally invariant systems, the shape of the momentum distribution can reveal several aspects of a many-body system, ranging from condensation to short-range correlations and spatial structure. In the present case, the hard-wall boundaries break translation invariance, such that the eigenstates of the system in the absence of interactions are given by the usual standing waves with quantized momentum $p_k = k\pi/L$, as mentioned above. In this section we present the occupation distribution in the single-particle space of those standing waves; we will refer to that distribution as the quasi-

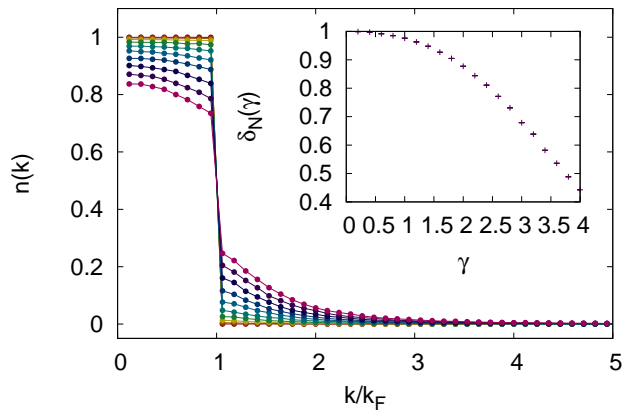


FIG. 6. Quasi-momentum distribution $n(k)$ for $N = 16$ particles as a function of $\gamma = 0.2, 0.6, 1.0, \dots, 3.8$ (top to bottom around $k = 0$), for $N_x = 80$. Inset: γ -dependence of the discontinuity δ_N in $n(k)$ at the Fermi surface. While δ_N could depend on N , our results for different N agree within our statistical and systematic uncertainties.

momentum distribution $n(k)$.

Figure 6 shows $n(k)$ per spin for a representative particle number $N = 16$, and for several couplings. For non-interacting systems, the ground-state distribution is the expected step function, with a unit discontinuity at the Fermi surface. As attractive interactions are turned on, pairing correlations begin to dominate, and the system progressively becomes more bosonic. This is clearly seen in the variation of the discontinuity δ_N in $n(k)$ as a function of γ : δ_N decreases monotonically as γ is increased. The inset of Fig. 6 shows $\delta_N(\gamma)$ for $N = 16$ particles. For the couplings studied here, it appears that $\delta_N(\gamma)$ decreases without a bound. However, it seems difficult to imagine a situation in which $\delta_N(\gamma) < 0$ and the energy is minimized. Under the assumption that that does not happen, we expect that $\delta_N(\gamma)$ approaches a non-negative constant asymptotically at large γ , i.e. the curve described by the data in the inset of Fig. 6 should eventually change convexity as it approaches a constant from above. To determine whether this conjecture holds, however, calculations in the strong-coupling, hard-core boson limit are needed [39].

E. Tan's contact density and contact

Short-range interactions, like the one studied here, induce correlations whose short-distance (high-momentum) form is encoded in Tan's contact [22]. Indeed, the short-distance dynamics is governed by the shape of the relative-coordinate wavefunction of the two-body problem, up to an overall factor that encapsulates many-body effects as well as effects due to external trapping potentials. The latter is the so-called contact C . One of the many ways to define the contact

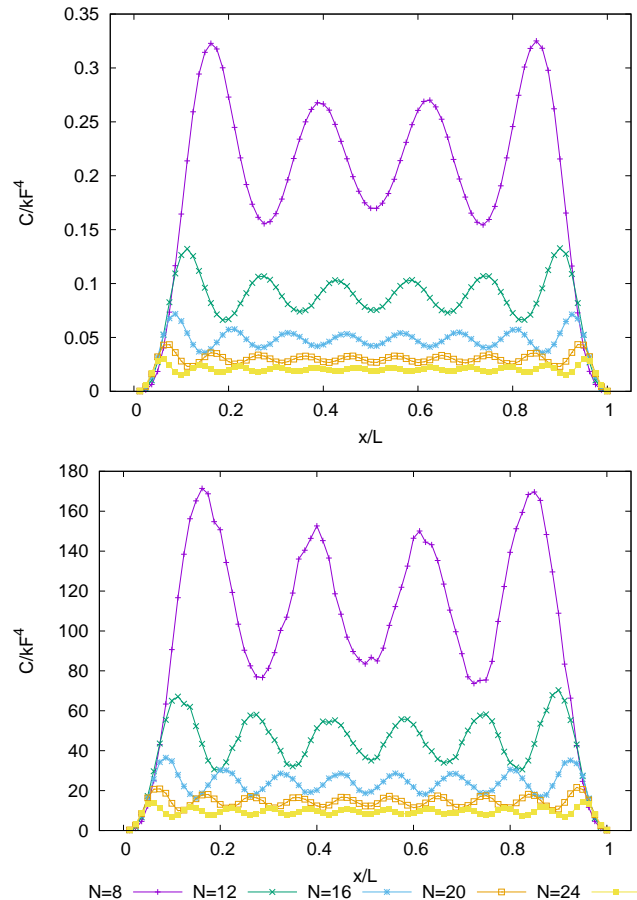


FIG. 7. Contact density $\mathcal{C}(x/L)$ as a function of the scaled position x/L for $N_x = 80$ at weak coupling ($\gamma = 0.2$, top panel) and strong coupling ($\gamma = 3.0$, bottom panel), for particle numbers $N = 8, 12, 16, 20, 24$ (top to bottom).

is through the Feynman-Hellmann theorem as applied to the variation of the ground-state energy with respect to the scattering length, which yields

$$C = -g\langle\hat{V}\rangle, \quad (30)$$

where $\langle\hat{V}\rangle$ is the ground-state expectation value of the interaction energy. Equation (3) indicates that C is given by an integral over the on-site correlation function among different spins, which for brevity we will call “contact density”. In our case, the presence of hard walls yields a spatially varying contact density $\mathcal{C}(x/L)$. Note that since g has units of inverse length (i.e. momentum), C has dimensions of inverse length cubed. Moreover, C is an extensive quantity. Therefore, below we use the intensive dimensionless form $C/(Nk_F^3)$; for the contact density we use $\mathcal{C}(x/L)/k_F^4$.

In Fig. 7 we show $\mathcal{C}(x/L)$ as a function of the scaled position x/L and in units of k_F^4 at two different couplings (top and bottom). In terms of number of peaks and valleys, the oscillations in $\mathcal{C}(x/L)$ follow the same pattern as those of the density $n(x/L)$. The amplitude varia-

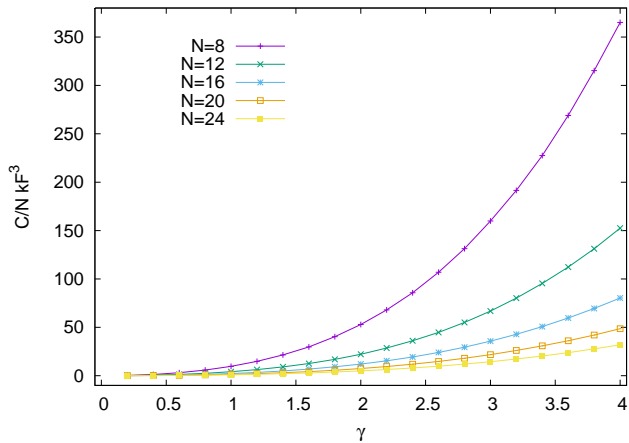


FIG. 8. Tan’s contact of $N = 8, \dots, 24$ unpolarized fermions in a 1D segment (discretized using $N_x = 80$ points), in units of its non-interacting counterpart E_{FG} , as a function of the dimensionless coupling γ .

tions are such that the minima are at roughly one half of the value of the maxima, regardless of coupling or particle number. While that trend remains as N is varied, the average value of $\mathcal{C}(x/L)/k_F^4$ away from the boundaries does seem to quickly approach a limit as N is increased, and the overall amplitude of the oscillations also decreases markedly. The integrated contact $\mathcal{C}/(Nk_F^3)$, shown in Fig. 8, also seems to approach the thermodynamic limit very quickly. This finding is in line with the observations of Ref. [36], which studied the few- to many-body progression of one-dimensional fermions with periodic boundary conditions.

IV. SUMMARY AND CONCLUSIONS

Studying systems with hard-wall boundaries via ultracold atoms is a way to access the behavior of the uniform-space limit, but when the boundaries are explicitly accounted for, it is also a different way to probe strongly coupled matter. In this work, we set out to characterize an elementary yet non-trivial many-body problem in that situation: spin-1/2 fermions with a zero-range interaction in a one-dimensional hard-wall box. We computed, in a fully ab initio fashion, the ground-state energy, density profiles, momentum distribution, and Tan’s contact density. Together, these quantities provide a basic yet comprehensive understanding of the effects of the boundaries and how they disappear in the thermodynamic limit. In short, we find that, upon scaling the density and the contact density by appropriate powers of k_F , the large- N limit is approached surprisingly quickly, as the largest

changes happen in the regime we studied, where $N = 8 - 24$.

The hard-wall boundaries lead to oscillating density profiles; such Friedel oscillations are characteristic not only of systems with interfaces but also of situations where an impurity is present. Our work clarifies the quantitative changes in the oscillation pattern due to short-range attractive interactions, which induce pairing correlations. We find that those effects are captured by a parametrization of the density which, while based on the noninteracting result, provides a remarkably clean way to understand the behavior of the density even in strongly coupled situations. We extended that analysis to the one-body density matrix, and further complemented it by computing the quasi-momentum distribution. The latter shows clear interaction effects as a change in the discontinuity at the Fermi surface.

Aside from the above, we calculated the ground-state energy (which we provide as a benchmark for other approaches and future studies) and the Tan contact density (i.e. on-site pairing correlations) which encode all of the short-distance behavior of response functions via the operator product expansion.

We carried out this work by discretizing space and (imaginary) time and using the auxiliary-field path-integral representation of the many-body problem. We estimated that path integral using stochastic methods, namely the hybrid Monte Carlo algorithm. Our study used lattices of up to $N_x = 80$ points and covered weakly to strongly interacting regimes in systems of up to $N = 24$ particles. This Monte Carlo approach is one of the few tools that, in one dimension, can provide fully non-perturbative and well-controlled access to the physics of strongly coupled matter.

Our work is a first step towards: a) exploring the detailed structure of two-body correlations, b) studying finite-temperature effects, and c) higher dimensions, including mixed-dimensions. Point b) is particularly important because finite-T effects are only cleanly accessible with exact diagonalization or with QMC, as the Bethe ansatz does not provide a controlled approximation in that case (at least not for all temperatures).

ACKNOWLEDGMENTS

We gratefully acknowledge discussions with D. Lee, T. Schäfer, and J. E. Thomas (NCSU), as well as with L. Rammelmüller (TU Wien and TU Darmstadt). This material is based upon work supported by the National Science Foundation under Grants No. PHY1306520 (Nuclear Theory Program) and PHY1452635 (Computational Physics Program).

[1] I. Bloch, J. Dalibard, and W. Zwerger, *Rev. Mod. Phys.* **80**, 885 (2008); S. Giorgini, L. P. Pitaevskii, and S.

Stringari, *Rev. Mod. Phys.* **80**, 1215 (2008); J. Levin-

- sen, M. M. Parish, *Annu. Rev. Cold Atoms Mol.* **3**, 1 (2015); *Ultracold Fermi Gases*, Proceedings of the International School of Physics “Enrico Fermi”, Course CLXIV, Varenna, June 20 – 30, 2006, M. Inguscio, W. Ketterle, C. Salomon (Eds.) (IOS Press, Amsterdam, 2008).
- [2] N.T. Zinner and A. S. Jensen, *J. Phys. G: Nucl. Part. Phys.* **40**, 053101 (2015).
- [3] I. Bloch, *J. Phys. B: At. Mol. Opt. Phys.* **38** S629 (2005); M. A. Cazalilla, A. M. Rey, *Rep. Progr. Phys.* **77**, 124401 (2014).
- [4] M. Mancini, G. Pagano, G. Cappellini, L. Livi, M. Rider, J. Catani, C. Sias, P. Zoller, M. Inguscio, M. Dalmonte, L. Fallani, *Science* **349**, 1510 (2015); B. K. Stuhl, H.-I. Lu, L. M. Aycock, D. Genkina, and I. B. Spielman, *Science* **349**, 1514 (2015).
- [5] A. L. Gaunt, T. F. Schmidutz, I. Gotlibovych, R. P. Smith, Z. Hadzibabic, *Phys. Rev. Lett.* **110**, 200406 (2013).
- [6] J. Friedel, *Philos. Mag.* **43** 153 (1952); *Nuovo Cim. Suppl.* **7**, 287 (1958).
- [7] I. Tütto and A. Zawadowski *Phys. Rev. B* **32**, 2449 (1985).
- [8] V. I. Fernández and C. M. Naón *Phys. Rev. B* **64**, 033402 (2001).
- [9] B. Chatterjee and K. Byczuk, *J. Phys.: Conference Series* **592**, 012059 (2015).
- [10] E. G. Dalla Torre, D. Benjamin, Y. He, D. Dentelski, and E. Demler, arXiv:1507.04345.
- [11] R. F. Zhang, A. S. Argon, and S. Veprek, *Phys. Rev. Lett.* **102**, 015503 (2009).
- [12] K. W. Clark, X.-G. Zhang, G. Gu, J. Park, G. He, R. M. Feenstra, and A.-P. Li, *Phys. Rev. X* **4**, 011021 (2014).
- [13] M. Bouhassoune, B. Zimmermann, P. Mavropoulos, D. Wortmann, P. H. Dederichs, S. Blügel, and S. Lounis, *Nature Comm.* **5**, 5558 (2014).
- [14] M. Fabrizio and A. O. Gogolin, *Phys. Rev. B* **51**, 17827 (1995).
- [15] R. Egger and H. Grabert, *Phys. Rev. Lett.* **75**, 3505 (1995).
- [16] G. Bedürftig, B. Brendel, H. Frahm, R. M. Noack, *Phys. Rev. B*, **58**, 10225 (1998).
- [17] D. Vieira, H. J. P. Freire, V. L. Campo Jr., and K. Capelle *J. Magn. Magn. Mater.* **320**, e418 (2008).
- [18] G. Xianlong *Phys. Rev. A* **86**, 023616 (2012).
- [19] Z. Xu, L. Li, G. Xianlong and S. Chen, *J. Phys.: Condens. Matter*, **25** 055601 (2013).
- [20] A. Angelone, M. Campostrini, and E. Vicari, *Phys. Rev. A* **89**, 023635 (2014).
- [21] S. A. Soeffing, M. Bortz, I. Schneider, A. Struck, M. Fleischhauer, S. Eggert, *Phys. Rev. B* **79**, 195114 (2009).
- [22] S. Tan, *Ann. Phys.* **323**, 2952 (2008); *ibid.* **323**, 2971 (2008); *ibid.* **323**, 2987 (2008); S. Zhang, A. J. Leggett, *Phys. Rev. A* **77**, 033614 (2008); F. Werner, *Phys. Rev. A* **78**, 025601 (2008); E. Braaten, L. Platter, *Phys. Rev. Lett.* **100**, 205301 (2008); E. Braaten, D. Kang, L. Platter, *ibid.* **104**, 223004 (2010).
- [23] X.J. Liu, *Phys. Rep.* **524**, 37 (2013).
- [24] C. E. Berger, E. R. Anderson, J. E. Drut, *Phys. Rev. A* **91**, 053618 (2015).
- [25] T. Grining, M. Tomza, M. Lesiuk, M. Przybytek, M. Mushiak, P. Massignan, M. Lewenstein, R. Moszynski *New J. Phys.* **17**, 115001 (2015).
- [26] C. E. Berger, J. E. Drut, W. J. Porter, *Comput. Phys. Commun.* (2016).
- [27] T. Giamarchi, *Quantum Physics in One Dimension*, (Oxford University Press, Oxford, 2004).
- [28] X.-W. Guan, M. T. Batchelor, and C. Lee, *Rev. Mod. Phys.* **85**, 1633 (2013).
- [29] T. Deguchi and R. Yue, arXiv:cond-mat/9704138
- [30] A. Imambekov, T. L. Schmidt, and L. I. Glazman, *Rev. Mod. Phys.* **84**, 1253 (2012).
- [31] A. Imambekov and L. Glazman, *Phys. Rev. Lett.* **102**, 126405 (2009); *Science* **323**, 228 (2009);
- [32] P. D’Amico and M. Rontani, *Phys. Rev. A* **91**, 043610 (2015).
- [33] E. J. Lindgren, J. Rotureau, C. Forssén, A. G. Volosniev, N. T. Zinner *New J. Phys.* **16**, 063003 (2014);
- [34] T. Sowiński, M. Gajda, K. Rzazewski, *EPL* **109**, 26005 (2015).
- [35] T. Sowiński, *Few-Body Syst.* **56**, 659 (2015).
- [36] L. Rammelmüller, W. J. Porter, A. C. Loheac, J. E. Drut *Phys. Rev. A* **92**, 013631 (2015).
- [37] F. F. Assaad and H. G. Evertz, *Worldline and Determinantal Quantum Monte Carlo Methods for Spins, Phonons and Electrons*, in *Computational Many-Particle Physics*, H. Fehske, R. Shneider, and A. Weise Eds., Springer, Berlin (2008); J. E. Drut and A. N. Nicholson, *J. Phys. G: Nucl. Part. Phys.* **40**, 043101 (2013);
- [38] S. Duane, A. D. Kennedy, B. J. Pendleton, D. Roweth, *Phys. Lett. B* **195**, 216 (1987); S. A. Gottlieb, W. Liu, D. Toussaint, R. L. Renken, *Phys. Rev. D* **35**, 2531 (1987).
- [39] A. G. Volosniev, D. V. Fedorov, A. S. Jensen, M. Valiente, and N. T. Zinner, *Nat. Commun.* **5**, 5300 (2014).